Geometry dependent model and analysis of the AR-CVT actuation

Geometry Dependent Model and Analysis of the AR-CVT Actuation

Jannis D.G. van Kerkhoven

DCT 2006.077

Traineeship report

Coach(es): dr.ir. Bas Vroemen

Supervisor: prof.dr.ir. Maarten Steinbuch

Technische Universiteit Eindhoven
Department Mechanical Engineering
Dynamics and Control Technology Group

Eindhoven, November, 2006

Contents

Chapter 1

Introduction

A simplified model of the AR-CVT would be a convenient tool in commercial designing processes. Especially a geometry and load dependent model such as presented in this report adds some interesting benefits to the design process. The model can be used as a standard for future design of an AR-CVT for any set of requirements giving the advantage of not having to go through the entire development process again.

Important for current and future design processes is gaining a good insight in the working principle of the AR-CVT. The model derived in this report provides the insight required for optimal design of the AR-CVT.

An analysis of the AR-CVT is also important for predicting the specifications of the actuation system.

First the geometry of the AR-CVT is analysed as well as the forces and power required to actuate the AR-CVT. Hereby a simplified, geometry dependent model is derived and analysed to show the influence of several geometrical properties of the AR-CVT. Accordingly the results are evaluated for a European Transient Cycle, which contains data concerning a commercial vehicle during a city cycle. Subsequently the parameters are changed to analyse their influence on for instance the actuation power and an optimal configuration is presented. Finally several constructive alternatives for the actuation system are discussed.

Since an extensive analysis of the axial movable pulley and the passive control by a torque sensor in being executed parallel to this analysis, this report focuses mainly on modeling and analysing the radial pulley and its active electromechanical actuation.

Chapter 2

Introduction to the CS-PTO and AR-CVT concepts

A CS-PTO is a Constant Speed Power Take-Off used mostly on commercial vehicles to drive auxiliaries. Energy efficient use of auxiliaries often demands a constant power supply while the engine speed goes through its entire range. A CS-PTO provides this constant output speed to drive for instance a cooling generator. The current CS-PTO uses an electromechanically actuated Continuously Variable Transmission or CVT to deliver a constant output speed for varying input speeds. The CVT has two axially moving pulleys, one actively controlled with an electric motor, the other passively controlled with a torque sensor. The current CS-PTO is limited in the amount of transmittable power, about 15 kW. In the near future however the power demand increases to 30 kW.

The main limitation of the current system is the use of a dry hybrid pull belt, incapable of transmitting the increased power and torque. Also the actuation will demand too much power for increasing output demands and another problem of the current system is the self-locking actuation. The latter could cause large problems. For instance if the engine speed is low and the actuation would fail the CVT would remain at the same transmission ratio. Now if the engine speed is increased this causes a cooling generator on the output shaft of the CS-PTO to rev up accordingly, which might, due to far too high rotational speeds, have destructive consequences for the generator. This is of course a situation to be avoided. Another problem is the principle of actuating a rotating pulley in axial direction since there is always a contact surface between the actuation and the pulley which causes high friction or unstable connections, for systems with higher output demands this problem is only becoming larger.

The AR-CVT concept is a possible solution for the problems that will occur with the current CS-PTO. AR-CVT stands for Axial Radial-CVT which refers to the moving directions of the two pulleys. In contradiction to the current system, only one pulley moves in axial direction and it is passively controlled by a torque sensor. The other pulley is mounted on a lever and is electromechanically actuated in radial direction. The pivoting point of the lever is the ingoing shaft of the CS-PTO, meaning the ingoing shaft remains fixed while the radial pulley is free to translate on an circular trajectory around the ingoing shaft. In Figure 2.1 the working principle of the AR-CVT is shown.

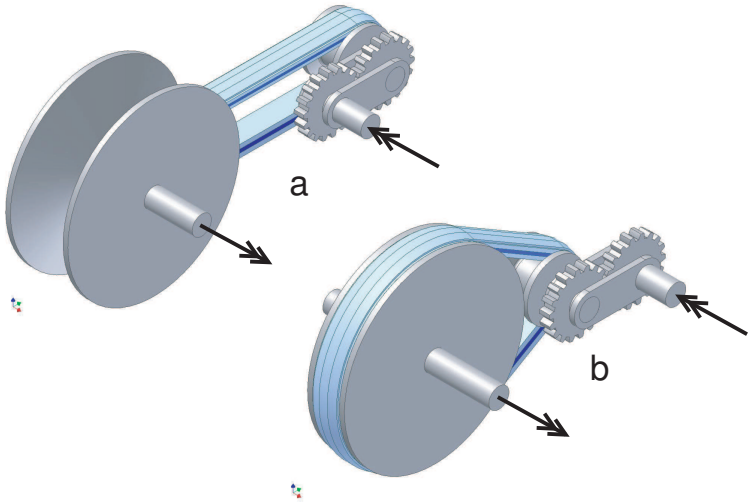

Figure 2.1: The AR-CVT for maximal (a) and minimal (b) transmission ratio (outgoing speed/ingoing speed)

The first problem with the current system is avoided by using a Van Doorne push belt, capable of transmitting far higher torque and power than a dry hybrid pull belt. Secondly the power required for actuation is to remain, at the most, equal to the current requirements to make the system commercially and technically interesting. Furthermore the problem of a self-locking system is taken into account in designing the actuation and finally the constructional problem of actively controlling a rotating pulley in axial direction is solved by actuating the pulley in radial direction from solid ground.

Chapter 3

Modeling the AR-CVT

3.1 Geometry

The dimensions of the AR-CVT are partially obtained from earlier research conducted by Jos den Ouden [1]. In fact by these prescribed geometrical properties, all system parameters are indirectly determined. The geometry and power analysis show that the geometry and position of the components are all a function of the ratio of the transmission, which in its turn is determined by merely the ingoing speed, or engine speed, because the outgoing speed should be constant at 3000 RPM.

In Figure 3.1 the AR-CVT is schematically represented. The right pulley has two pulley flanges moving axially and by doing so the radius on this pulley R_a varies. This pulley is referred to as the axial pulley. The left pulley translates in radial direction resulting in a change in the center distance a_h and is referred to as the radial pulley. For low engine speeds the transmission ratio r, defined as outgoing speed/ingoing speed, is maximal, the radius R_a is minimal and the center distance a_h maximal (solid). For high engine speeds the ratio is minimal, R_a maximal and a_h minimal (dashed). These two extreme situations are shown in Figure 3.1, in reality the position of the radial pulley differs, since the trajectory of the pulley is circular around the ingoing shaft and not linear as could be interpreted from the Figure. The center distance a_h however is the same. R_a and a_h are only

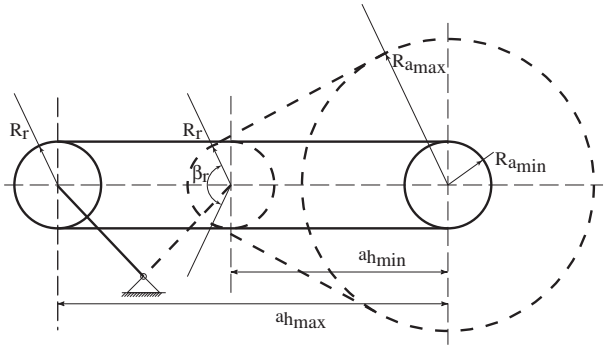

Figure 3.1: Simplified overview of the AR-CVT

dependent on each other, since all other parameters are prescribed by geometrical boundaries such as the fixed belt length and radius R_r. A relation between R_a and a_h can be derived, and in addition their time derivatives. The relation between R_a and a_h is used to determine the forces acting on the radial pulley at a certain transmission ratio r and thus at certain R_a and a_h. The time derivatives of R_a and a_h are used to analyse the power that is required to actuate the radial pulley sufficiently fast.

The center distance between the two pulleys a_h can be written as a function of the geometry of the belt transmission [2]:

$$a_h = \frac{L - R_r\beta_r - R_a\left(2\pi - \beta_r\right)}{2\sin\left(\frac{\beta_r}{2}\right)} \tag{3.1}$$

Where L is the length of the Van Doorne push belt, R_r the fixed radius of the radial pulley, R_a the variable radius of the axial pulley, β_r the angle of wrap on the radial pulley and $(2\pi - \beta_r)$ the angle of wrap on the axial pulley. The angle of wrap on the radial pulley can be written as [2]:

$$\beta_r = 2\cos^{-1}\left(\frac{R_a - R_r}{a_h}\right) \tag{3.2}$$

Replacing (3.2) in (3.1) results in a relation where a_h and R_a are the only variables:

$$a_h = \frac{L - 2R_r\cos^{-1}\left(\frac{R_a - R_r}{a_h}\right) - 2R_a\left(\pi - \cos^{-1}\left(\frac{R_a - R_r}{a_h}\right)\right)}{2\sqrt{1 - \frac{(R_a - R_r)^2}{a_h^2}}} \tag{3.3}$$

Note that a_h is not an explicit function of R_a. This equation cannot be solved analytically, so solutions for a_h are found by implementing the equation in MATLAB and using a zero finder for certain values of R_a, where the values of R_a are obtained from the research of Jos den Ouden [1] and shown in Table 3.1. For the entire range of R_a, a_h can now be determined since a certain engine speed, requires a certain transmission ratio to keep the outgoing speed at 3000 RPM, indicating a certain R_a since R_r is fixed. The extreme values of a_h are presented in Table 3.1

To determine the velocity of the radial pulley, needed for power calculations, the time derivative of a_h is to be calculated. The time derivative of a_h equals the velocity of the radial pulley along the center line of the two pulleys v_{rp}, where a positive velocity indicates an increase of a_h. Since a_h itself is not a function of time but there does exist time dependency of R_a, the partial time derivative of a_h is written as:

$$\dot{a_h} = \frac{\delta a_h}{\delta R_a}\frac{\delta R_a}{\delta t} \tag{3.4}$$

Here merely the partial derivative $\delta a_h/\delta R_a$ is evaluated. The time derivative of R_a is discussed in Chapter 4 since additional data concerning the rate of change of the engine speed is needed. Again it is very difficult to analytically determine da_h/dR_a,

so to find a solution, first the relation between a_h and R_a is approximated using a fitter in MATLAB. The fitter uses a polynomial relation:

$$a_h = p_0 + p_1 R_a + p_2 R_a^2 \tag{3.5}$$

This second order fit results in a maximal approximate error in a_h of $4 \cdot 10^{-4}$ m. Considering a_h to be of order 10^{-1} m this is sufficiently accurate to describe the relation between a_h and R_a. It is now fairly simple to determine $\delta a_h / \delta R_a$.

$$\frac{\delta a_h}{\delta R_a} = p_1 + 2 p_2 R_a \tag{3.6}$$

The results for both a_h and $\delta a_h / \delta R_a$ are plotted in Figure 3.2, where the upper graph shows the calculated values of a_h and the lower graph shows the approximated values of $\delta a_h / \delta R_a$.

$R_{a_{min}}$	=	$30 \cdot 10^{-3}$ [m]
$R_{a_{max}}$	=	$101 \cdot 10^{-3}$ [m]
$a_{h_{min}}$	=	$151 \cdot 10^{-3}$ [m]
$a_{h_{max}}$	=	$279 \cdot 10^{-3}$ [m]
R_r	=	$30 \cdot 10^{-3}$ [m]

Table 3.1: Basic dimensions of the AR-CVT

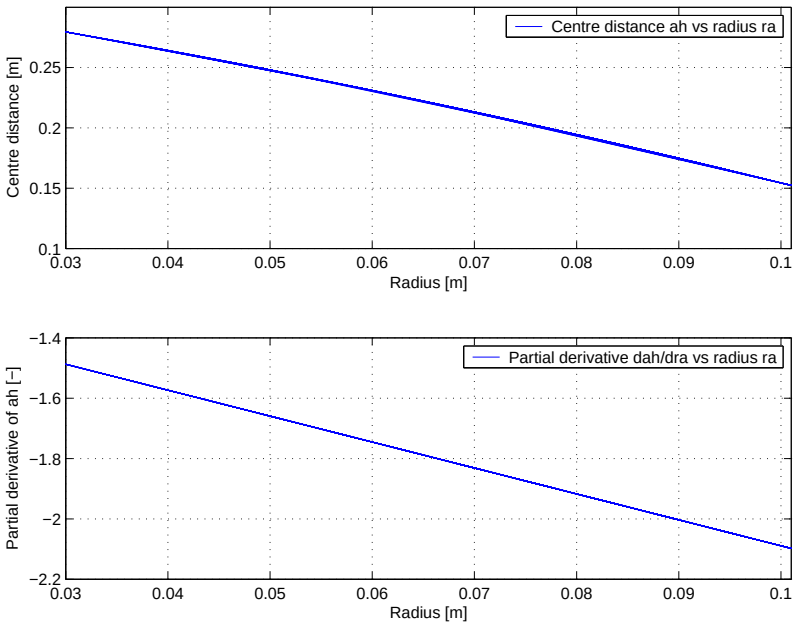

Figure 3.2: Values of a_h and da_h / dR_a for the entire range of R_a

3.2 Forces

In this section a simplified model is obtained for the forces that act on the components of the AR-CVT. The starting point hereby is the assumed constant load torque at the outgoing shaft. This load causes the passive controller - i.e. a torque sensor in the axial pulley - to generate a clamping force on the two pulley flanges. The push belt is squeezed and, due to the wedge angle of the pulley flanges, pushed out of the pulley. Because the radial pulley is held in a fixed position, this generates tension forces in the push belt. In other words one can say that the clamping force is transferred to the radial pulley through the tension forces in the belt. Secondly the load torque is transferred to the push belt by friction between the belt and the pulley flanges and subsequently the torque is transmitted to the radial pulley by compression forces in the push belt. To calculate the forces in the belt we make some assumptions:

- all load torque is transferred by the compression forces in the belt which are linearly built up along the angle of wrap by tangential friction.
- the tension forces in both the compressed and the slack part of the push belt are assumed equal for the friction between the belt bands and belt segments is neglected.
- the clamping force in the axial pulley is distributed uniformly along the angle of wrap.
- the tangential components of the friction force, responsible for torque transfer, between the push belt and the pulley flanges is distributed uniformly along the angles of wrap on both the radial and the axial pulley.
- the radial component of the friction between the pulley flanges and the push belt is neglected, for it is very small compared to the tangential component of friction.
- furthermore losses in and between the belt and pulleys are neglected.
- Also centrifugal forces on the push belt are neglected.

Considering the uniform distribution of the friction and clamping forces first the forces on a single belt element are discussed. Force equilibriums on the axial pulley and the belt are used to determine the forces on the radial pulley. As mentioned the load torque is assumed to be constant, in table 3.2 values are given for the demands as they currently exist for the output of the AR-CVT.

$T_a =$	96	[Nm]	Maximal Load Torque
$P_a =$	30	[kW]	Maximal Output power
$w_a =$	3000	[Rpm]	Maximal Output angular speed

Table 3.2: Output requirements of the AR-CVT

3.2.1 Forces on the push belt

The forces acting on a single segment are shown Figure 3.3 which, because of symmetry, shows only half a single segment. As mentioned above the tension forces in the belt are caused by the clamping force F_{clamp} in the axial pulley, subsequently causing a radial force F_{rad} distributed along the angle of wrap. Considering the symmetry of the segments we can write for the forces on a single segment in radial direction:

$$dF_{rad} = 2\tan(\theta)dF_c \tag{3.7}$$

Where θ is the pulley wedge angle and dF_c is the axial clamping force per unit of angular width. Note that dW_{rad} is neglected since it is assumed to be very small in comparison to the radial force on each component dF_{rad} and the friction in tangential direction dW_{tan} [3]. Since the friction between the belt segment and bands is neglected, the internal belt forces are of no interest. The only forces of interest are then the normal and tangential friction forces dN and dF_c (i.c.w. neglecting the radial friction dW_{rad}) . Thus the contribution of Q and $Q + dQ$ to dF_{rad} is neglected. dF_{rad} determines dN preventing the belt being pushed out of the pulley. The tension forces F_{s_1} and F_{s_2} then transmit the forces to the other pulley resulting in a horizontal force F_{hor} on the radial pulley (Figure 3.4).

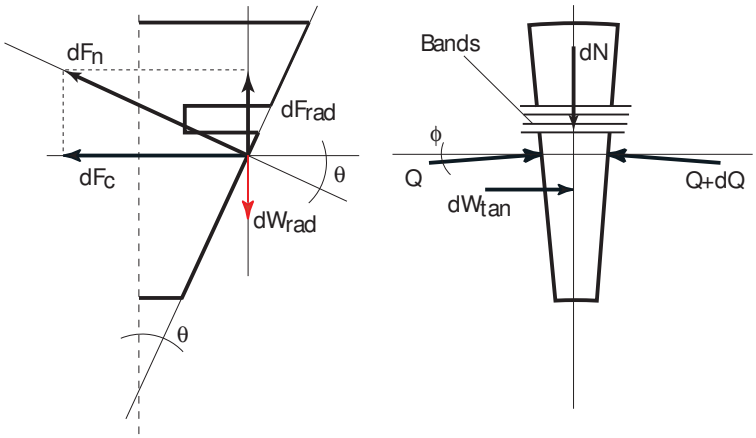

Figure 3.3: Forces per unit angular width, front view (left) and side view (right)

Since the total clamping force is assumed to be distributed uniformly over the angle of wrap, the clamping force per unit of angular width dF_c can be determined by dividing F_{clamp} over the angle of wrap on the axial pulley $(2\pi - \beta_r)$. The angular width of a segment is assumed to be $d\epsilon$. The clamping force per segment is then written as:

$$dF_c = \frac{F_{clamp}}{(2\pi - \beta_r)} d\epsilon \tag{3.8}$$

To evaluate the total of radial forces that cause the tension forces F_{s_1} and F_{s_2}, the effective angle of wrap on the axial pulley is introduced. In Figure 3.4 one can see that in the shaded area on the pulley, between β_r and $(2\pi - \beta_r)$, the radial

forces counter act one another. One might say that the forces in this area are not 'effective' implying that the effective angle of wrap on the axial pulley equals β_r.

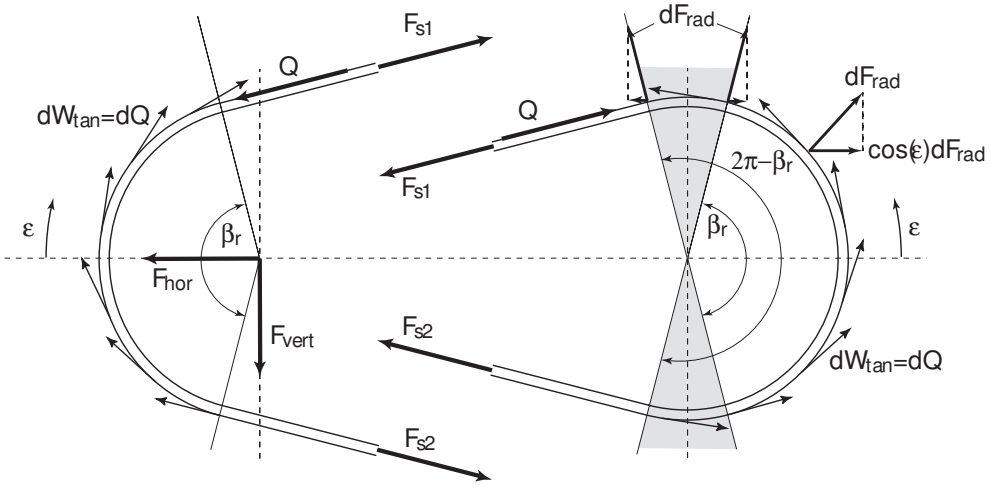

Figure 3.4: Forces on the push belt caused by the load and output torque resulting in equilibrium forces F_{hor} and F_{vert} on the radial pulley

The 'vertical' components of the radial forces counter act each other not only outside the effective angle of wrap, in fact they do so over the entire angle of wrap. So the focus is merely on the horizontal parts of dF_{rad}. From Figure 3.4 it can be seen that for the 'horizontal' components can be written:

$$\begin{aligned} dF_{rad_{hor}} &= dF_{rad}\cos(\epsilon) \\ &= 2\tan(\theta)dF_c\cos(\epsilon) \\ &= 2\tan(\theta)\frac{F_{clamp}}{(2\pi-\beta_r)}\cos(\epsilon)d\epsilon \end{aligned} \tag{3.9}$$

Where the 'horizontal' is the center line between the two pulleys. The total horizontal force $F_{rad_{hor}}$ on the belt resulting from the axial clamping force is now obtained by integrating 3.9 over the effective angle of wrap:

$$\begin{aligned} \Sigma F_{rad_{hor}} &= 2\int_0^{\frac{1}{2}\beta_r} 2\tan(\theta)\frac{F_{clamp}}{(2\pi-\beta_r)}\cos(\epsilon)d\epsilon \\ &= 4\tan(\theta)\frac{F_{clamp}}{(2\pi-\beta_r)}\sin(\frac{1}{2}\beta_r) \end{aligned} \tag{3.10}$$

Furthermore in the side view in Figure 3.3, Q and $Q+dQ$ are the compression forces between successive segments and dW_{tan} is the tangential component of friction between a segment and the pulley, while dW_{tan} equals the compression force between segments dQ since ϕ is small. Due to uniformly distributed axial clamping force, the transmitted torque is assumed to build up linearly along the

angle of wrap. We can write dQ as a function of the total compression force Q and per unit of angular width. Note that dQ is evaluated over the part of the belt on the radial pulley instead of the axial pulley since it is the forces on the radial pulley we are interested in. For the increase in compression force per segment along the angle of wrap dQ can be written:

$$dQ = \frac{Q}{\beta_r} d\epsilon \tag{3.11}$$

Where Q is the total uniformly distributed compression force easily determined from the load torque by $Q = T_a/R_a$. Considering a uniform distribution of the tangential friction components, the 'horizontal' parts of $dW_{tan} = dQ$ counter act each other. So concentrating on the vertical parts of dQ we integrate (3.11) over the angle of wrap on the radial pulley:

$$\begin{aligned} dQ_{vert} &= dQ\cos(\epsilon) \\ dQ_{vert} &= \frac{Q}{\beta_r}\cos(\epsilon)d\epsilon \\ \Sigma dQ_{vert} &= 2\int_0^{\frac{1}{2}\beta_r} \frac{Q}{\beta_r}\cos(\epsilon)d\epsilon \\ &= 2\frac{Q}{\beta_r}(\sin(\frac{1}{2}\beta_r) - 1) \end{aligned} \tag{3.12}$$

From Figure 3.4 it can be seen that there are two forces required two obtain force equilibrium on the push belt. A horizontal force F_{hor} resulting from the clamping force on the axial pulley transmitted to the push belt by $\Sigma F_{rad_{hor}}$ and through the push belt by F_{s1} and F_{s2}. A vertical component F_{vert} resulting from the load torque on the radial pulley transmitted to the push belt by $dW_{tan} = dQ$ and through the push belt by Q:

$$\begin{aligned} F_{hor} &= 4\tan(\theta)\frac{F_{clamp}}{(2\pi - \beta_r)}\sin(\frac{1}{2}\beta_r) \\ F_{vert} &= 2\frac{Q}{\beta_r}(\sin(\frac{1}{2}\beta_r) - 1) \end{aligned} \tag{3.13}$$

3.2.2 Forces on the radial pulley

Now two of the three main forces on the radial pulley are known. From Figure 3.5 it can be seen that the third major force on the radial pulley is the input torque. This torque is transmitted to the radial pulley by a spur gear mounted to the radial pulley shaft. The force that is caused by this this is determined by R_i the radius of the spur gear. The input torque always works tangential to the actuation arm, while the angle of F_{hor} and F_{vert} with the actuation arm changes when the radial pulley

pivots. Furthermore it can be seen from equation (3.13) that the magnitudes of F_{hor} and F_{vert} are dependent on the angle of wrap on the radial pulley β_r and therefore determined by a_h and R_a. Two forces keep the radial pulley in place: a reaction force F_{lever} in the direction of the arm and the actuation force F_{act} tangential to the arm. F_{act} is the most relevant for it is the amount of force required to hold and actuate the radial pulley while F_{lever} is compensated by the stiffness of the actuation arm and bearing.

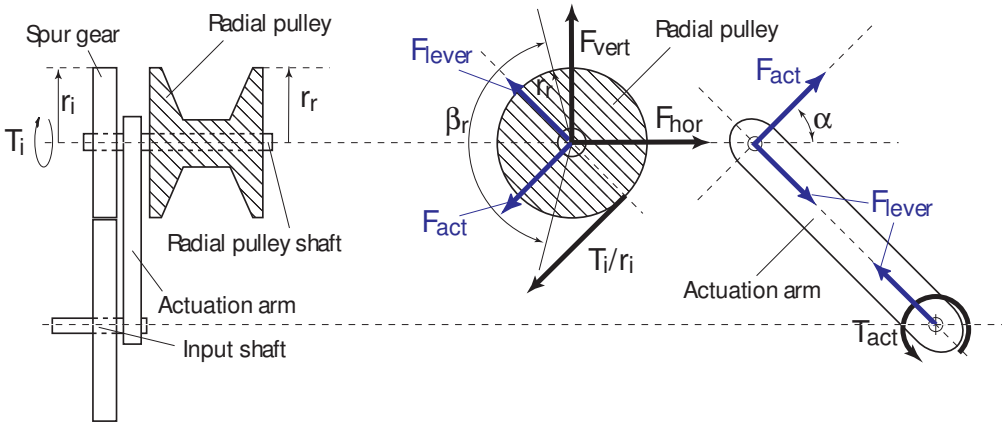

Figure 3.5: A schematic view of the radial pulley/spur gear/actuation arm for *clockwise rotation* of the radial pulley

To determine F_{act} an insight in the angles that the forces F_{hor} and F_{vert} make with the arm is required. In Figure 3.5 one can see that there is one angle of importance, the angle between F_{hor} and the pulley heart line: α. This angle changes when the radial pulley moves along its trajectory and, since it is determined by the geometry the can be expressed in a_h and R_a.

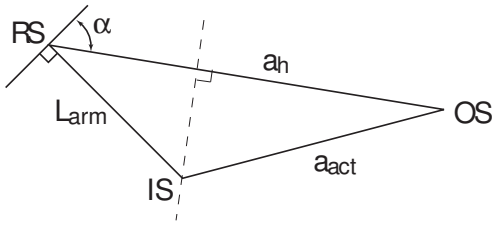

Figure 3.6: Schematic overview of the dimension of the AR-CVT

In Figure (3.6) one can see a schematic overview of the geometry of the AR-CVT. RS is the radial pulley shaft, OS the axial pulley or output shaft and IS the input shaft. Furthermore L_{arm} is the length of the actuation arm, a_h the pulley center distance and a_{act} the distance between the axial pulley shaft and the input shaft. The cosine rule is used to express α as a function of the geometry:

$$a_{act}^2 = a_h^2 + L_{arm}^2 - 2a_h L_{arm} \cos\left(\frac{1}{2}\pi - \alpha\right) \tag{3.14}$$

Since $\cos\left(\frac{1}{2}\pi - \alpha\right) = \sin(\alpha)$ equation (3.14) can be rewritten as:

$$a_{act}^2 = a_h^2 + L_{arm}^2 - 2a_h L_{arm} \sin(\alpha) \tag{3.15}$$

From which α can be isolated:

$$\alpha = \sin^{-1}\left(\frac{a - act^2 - a_h^2 - L_{arm}^2}{-2a_h L_{arm}}\right) \tag{3.16}$$

Since F_{lever} is supported by the arm itself, only F_{act} is of interest. Force equilibrium around the radial pulley center gives for the actuation force:

$$F_{act} = \cos(\alpha)F_{hor} - \frac{T_i}{r_i} + \sin(\alpha)F_{vert} \tag{3.17}$$

The torque that is required to hold and move the radial pulley can be calculated from:

$$T_{act} = F_{act} L_{arm} \tag{3.18}$$

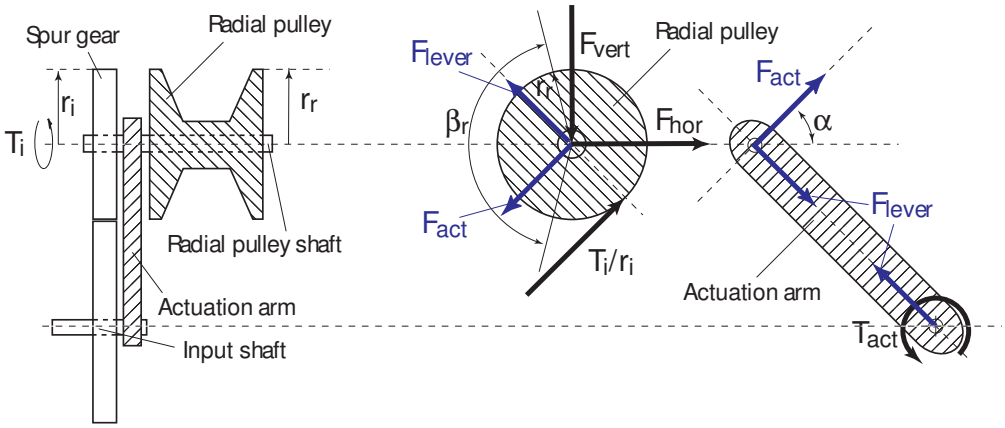

Figure 3.7: A schematic view of the radial pulley/spur gear/actuation arm for *counter clockwise rotation* of the radial pulley

Furthermore the direction of rotation of the AR-CVT has a significant influence on the required actuation force. In Figure 3.5 the forces were shown for clockwise rotation of the radial pulley. In Figure 3.7 the forces are shown for counterclockwise rotation. When switching the direction of rotation the direction of the input torque is mirrored with respect to the longitudinal of the actuation arm and the direction of the vertical force is mirrored with respect to the pulley center line. Equation (3.17) describes the forces for clockwise rotation of the radial pulley. For counterclockwise rotation of the radial pulley (3.17) becomes:

$$F_{act} = \cos(\alpha)F_{hor} + \frac{T_i}{r_i} - \sin(\alpha)F_{vert} \tag{3.19}$$

Equations (3.17) and (3.19) describe the dependency of the forces on the ratio r, via R_a, and the geometry, via L_{arm} and a_{act}. The optimization of these parameters is discussed in Chapter 5. To show the variation of the forces over the range of R_a some dimensional assumptions are made. These are shown in Table 3.3.

θ	= 11	[Degrees]	Half axial pulley wedge angle
F_{clamp}	= 20	[kN]	Maximal Clamping force
R_i	= 30	[mm]	Radius at which the ingoing torque acts
L_{arm}	= 100	[mm]	Length of the actuation arm
a_{act}	= 200	[mm]	Input/output shaft distance

Table 3.3: Parameters of the AR-CVT used to calculated the forces on the pulleys and the required actuation torque

In Figure 3.8 the actuation force is shown for both rotational directions. Note that the contribution to F_{act} of the vertical force, $sin(\alpha)F_{vert}$, becomes negative about halfway the trajectory of the radial pulley. This is due to the fact that there is a switch between supporting and counteracting the actuation force F_{act} halfway the trajectory.

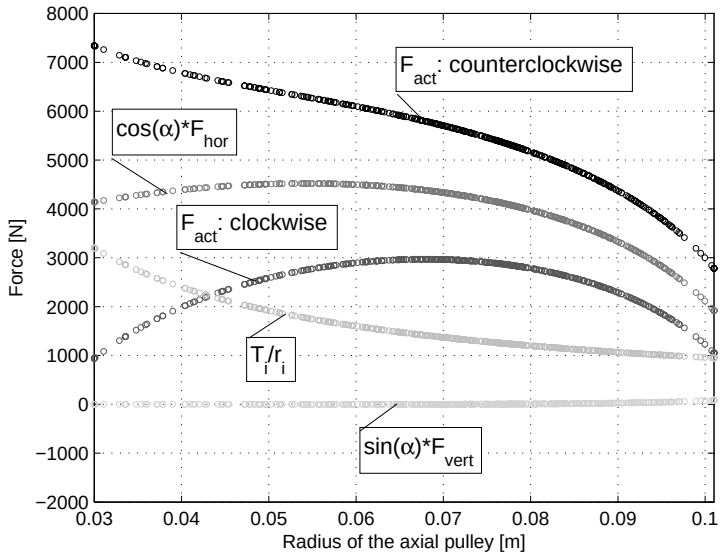

Figure 3.8: Force components tangent to the actuation arm and required actuation force F_{act} for both rotational directions

3.3 Power

The required power to actuate the radial pulley is now determined rather easily. It is obvious that the actuation power can be written as:

$$P_{act} = F_{act} v_{act} \tag{3.20}$$

Where v_{act} is the component of the pulley velocity tangential to the actuation arm. For v_{act} we write:

$$v_{act} = \frac{\dot{a_h}}{\cos(\alpha)} \tag{3.21}$$

So for clockwise rotation we write:

$$P_{act} = \left(\cos(\alpha) F_{hor} - \frac{T_i}{r_i} + \sin(\alpha) F_{vert} \right) \frac{\dot{a_h}}{\cos(\alpha)} \tag{3.22}$$

and for counterclockwise rotation:

$$P_{act} = \left(\cos(\alpha) F_{hor} + \frac{T_i}{r_i} - \sin(\alpha) F_{vert} \right) \frac{\dot{a_h}}{\cos(\alpha)} \tag{3.23}$$

Values for P_{act} are presented in Chapter 4 since at this stage the required shift rate, which determines $\dot{a_h}$, is not known.

3.4 Model validation

Earlier research conducted by Bas Vroemen on conventional CVT's resulted in a complex static model. A horizontal force is obtained from these calculations which corresponds to F_{hor} used in this model:

$$F_{hor_{Vr}} = 6.1 \cdot 10^3 + 1.3 \cdot 10^4 R_a \tag{3.24}$$

As can be seen from Figure 3.9 $F_{hor_{Vr}}$ is significantly higher than F_{hor}.

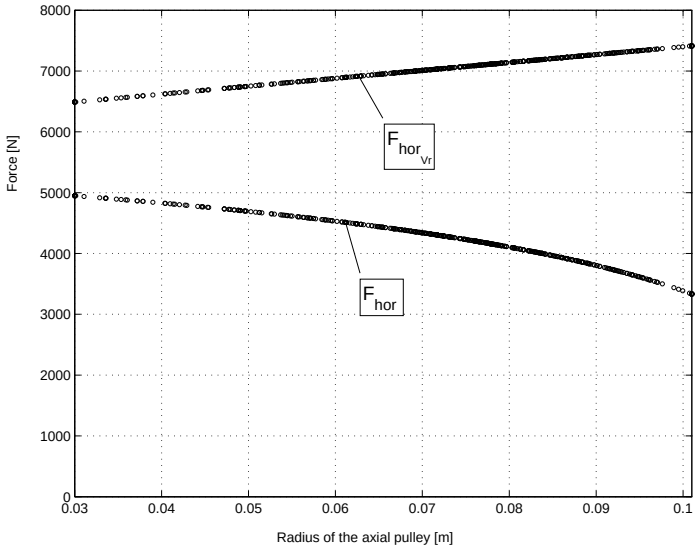

Figure 3.9: Comparison between F_{hor} and the corresponding force from a complex model

The figure above indicates that some of the made assumptions are not justified. Herein the assumptions of homogenous distribution of the clamping and friction forces are the most probable cause for the difference in the obtained results. In the model of Bas Vroemen complex integrals are used to calculate the build-up of torque along the angle of wrap, where in the simplified model this build-up is assumed to be linear. Also the parts of the angle of wrap where torque and friction forces are build up don't agree with the assumptions made. Furthermore the strict separation between the friction that causes the compression force Q, used only to calculate F_{vert} and the clamping force, used to calculate F_{hor}, causes deviations. The build-up of the compression along the angle of wrap may well contribute to the radial force on each segment, and thus to F_{hor}, and the non-linear build-up of the clamping force along the angle of wrap may well cause the belt tension in the slack and compressed part to deviate, thus contributing to F_{vert}. Also the assumption of linear build-up of compression forces causes deviations. The assumptions neglects the presence of a so called idle arc which in reality has a fairly large contribution to the distribution of torque build-up aling the angle of wrap [3].

However, the direction of the horizontal force in the complex model differs barely from the direction of F_{hor} in the simplified model. The direction of F_{hor} is assumed to be on the center line of the pulleys and $F_{hor_{Vr}}$ deviates no more than three degrees from this center line for all transmission ratios. Furthermore from Figure 3.8 it can be seen that the contribution of the vertical force component F_{vert} to the actuation force F_{act} is small. Obviously the ingoing torque is equal in both models. The remaining calculations in this report are made with an adjusted F_{hor} based on Vroemen's model resulting in the forces shown in Figure 3.10.

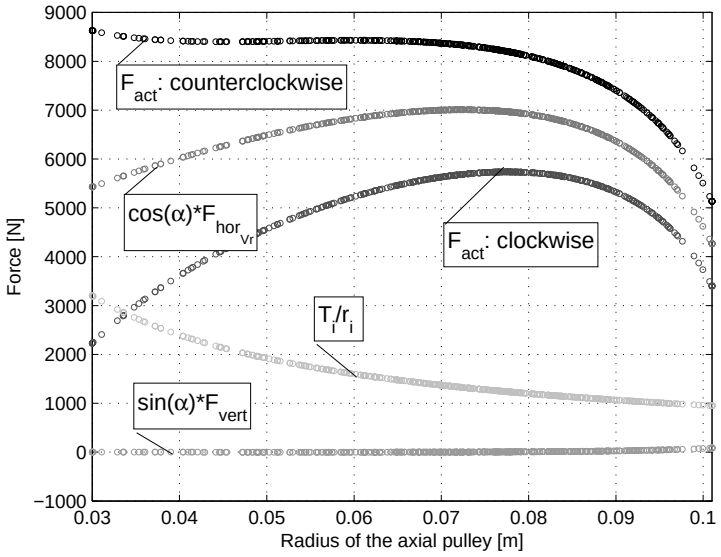

Figure 3.10: Forces on the radial pulley adjusted for Vroemen's model

Chapter 4

AR-CVT on a European Transient Cycle

Considering the fact that the AR-CVT will be used to drive refrigerant devices on commercial vehicles, it is assumable that the AR-CVT is applied mainly in city environments. A European Transient Cycle (ETC) is used to analyse a commercial vehicle engine speed on a ten minute city tour. From the engine speed change rate the required shift rate $\dot{R}_a$ can be determined, which is subsequently used to determine the required actuation power.

The ETC has a duration of 600 seconds. Every second a data point is recorded containing the engine speed which is evaluated to obtain the change rate of the engine speed. Since for every value of the engine speed a particular ratio is required to maintain a constant output speed, the ratio r can be determined for all 600 seconds. Accordingly the time derivative of R_a, i.e. the required shift rate $\dot{R}_a$, is incrementally ($\triangle t = 1$) determined (note that for an accurate determination of the shift rate, the sample frequency should be much higher than 1 Hz):

$$\dot{R}_a = \left.\frac{dR_a}{dt}\right|_{t=n} = \frac{R_{a_n} - R_{a_{n-1}}}{\triangle t} \tag{4.1}$$

According to equations (3.4), (3.22) and (3.23) the shift rate is used to determine the required actuation power. In Figure 4.1 the time derivative of R_a is shown for the entire ETC. Note that for the same radius R_a different shift rates can occur. Most of the time the shift rate is of small magnitude and most shifting during a city tour occurs at radii between $60 \cdot 10^{-3}$ m and $80 \cdot 10^{-3}$ m. Within this range also occur the highest shift rates of about $35 \cdot 10^{-3}$ m/s. Considering a radius range of about $70 \cdot 10^{-3}$ m the entire ratio range is reached in 2 seconds.

Using the same assumed values for L_{arm} and a_{act} as in section 3.2.2 the required actuation power is evaluated for an ETC. Here the forces are used as calculated in Chapter 3, thus Figure 4.2 gives an impression of the distribution of the actuation power. Again it can be seen that most of the time the radial pulley is nearly static in one position.

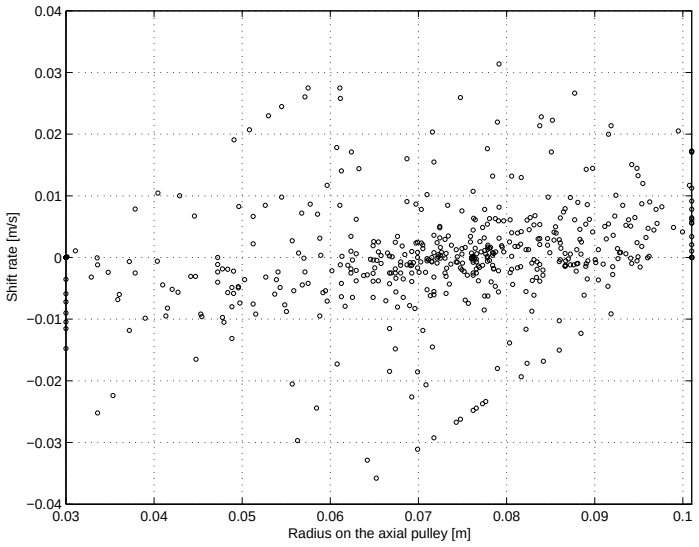

Figure 4.1: Shift rates, $\dot{R}_a$, on an ETC

Furthermore power is calculated for clockwise rotation of the radial pulley. Negative values of the power, due to negative velocities, are neglected. The actuation requires power only for holding the radial pulley in place and upshifting (increasing r, decreasing R_a, increasing a_h). Downshifting is achieved by merely releasing the actuation arm and thus requires no power. Note that for this system upshifting occurs at decreasing engine speed i.e. the transmission ratio r decreases for increasing engine speed.

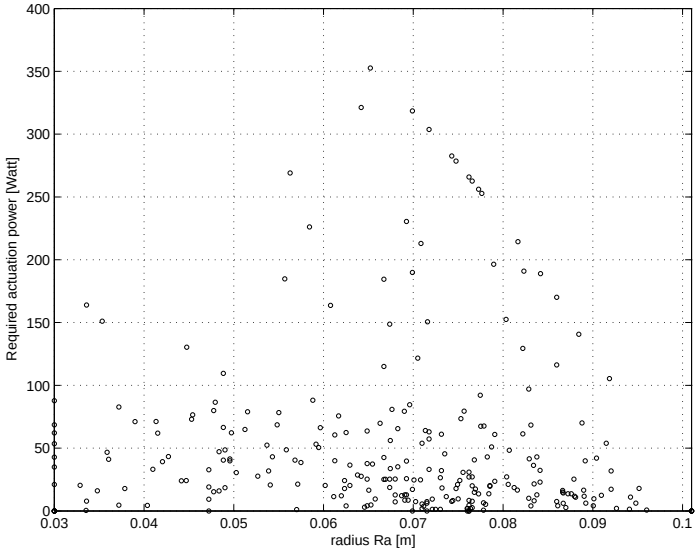

Figure 4.2: Required actuation power during an ETC

Chapter 5

Geometrical Optimization

From Chapter 3 it follows that the magnitudes of the forces are determined by the geometrical properties of the AR-CVT. Here an analysis is made of the influence of those properties on the forces. An optimum is sought for the one combination of dimensions that results in the lowest actuation power and torque. In addition to the geometrical dependency of the forces the direction of rotation is of great influence on the magnitude of the forces for certain pulley positions. Therefore first a choice is made between the two directions of rotation.

5.1 Direction of rotation

Actually only one argument is decisive in this matter. From Figures 3.5 and 3.7 one can see that the ingoing torque T_i can either support or counteract the actuation force (this holds for both the simplified and Vroemen's model). To keep the actuation force as low as possible we choose the direction of rotation to be clockwise for it results in a lower actuation force.

5.2 Geometrical configuration

To find an optimum configuration of geometrical properties, three dimensions are varied, namely the length of the actuation arm L_{arm}, the distance between the actuation shaft and the outgoing shaft a_{act} and the radius of the gear transmitting the ingoing torque to the radial pulley R_i. Where L_{arm} and a_{act} are only possible in certain combinations. They determine one another because of the fixed belt length and pulley radii (or radius range), R_i can be chosen within a certain range independent of the two former. First we look at L_{arm} and a_{act}.

The evaluated geometrical configurations are shown in Figure 5.1. One can see that for very large a_{act}, the limiting factor is the length of the arm which has to have a certain minimal length to let the radial pulley pivot from maximal a_h to minimal a_h. For smaller a_{act} the push belt of the AR-CVT becomes a critical factor because insufficient arm length will cause the input shaft to collide with the belt. The numbers in the figure indicate the position of the actuation shaft and the corresponding trajectory of the radial pulley shaft.

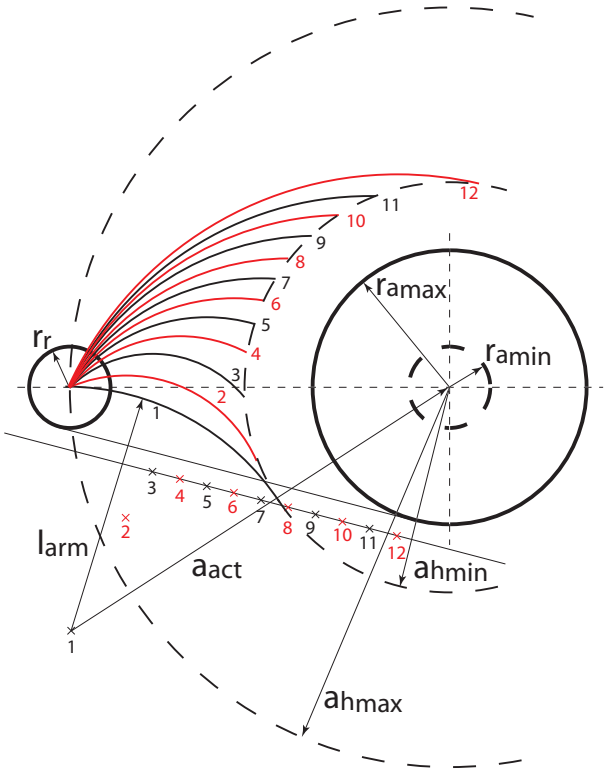

Figure 5.1: Different geometrical configurations

The positions shown in Figure 5.1 are chosen to be of practical value, considering the final outside dimensions of the AR-CVT, and the requirement that the trajectory of the radial pulley includes maximal and minimal a_h. In other words, for each evaluated a_{act} the arm length is minimized. For each position the actuation torque is calculated. These torques are shown in Figure 5.2. In addition each configuration the maximal required actuation power is calculated and shown in Figure 5.3. In these calculations R_i is assumed equal to the radial pulley radius R_r.

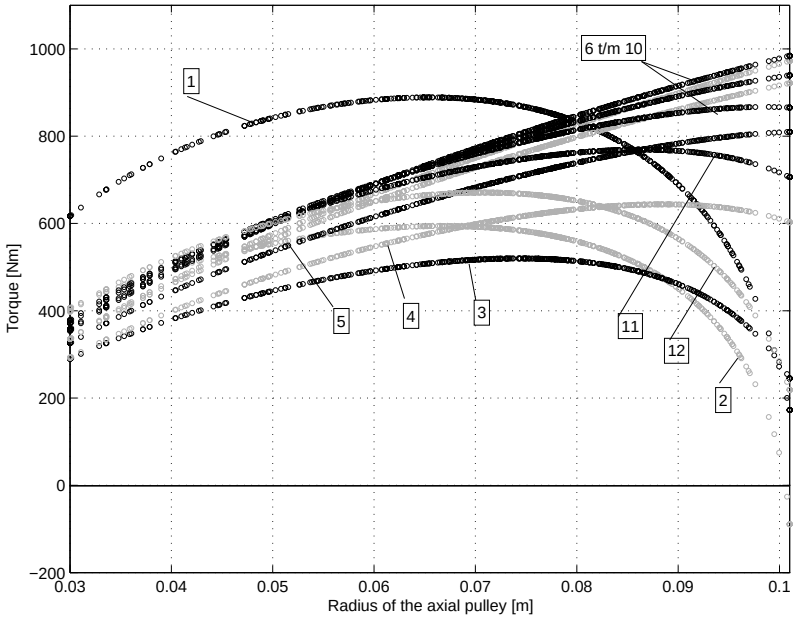

Figure 5.2: Required actuation torque T_{act} vs the axial pulley radius R_a for different geometrical configurations

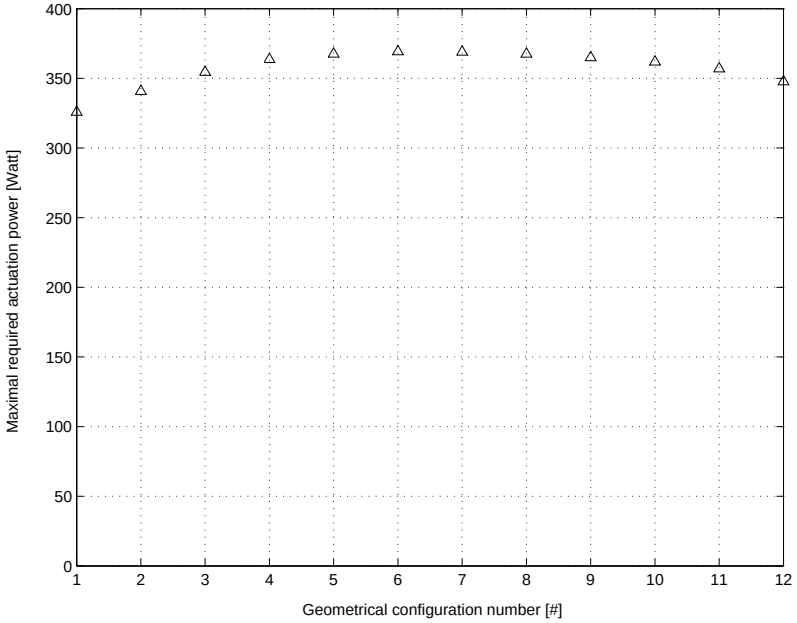

Figure 5.3: Required actuation power P_{act} for different geometrical configurations

Looking at Figures 5.2 and 5.3 one can see that configuration number 3 results in the lowest actuation torque. The lowest actuation power, although the differences are fairly small, occurs in configuration 1, while the torque is very large due to a long actuation arm. Considering the practical use of the AR-CVT the position of the input shaft is designed as close to configuration 3 as possible. This configuration results in the smallest dimensions and the required actuation power is very acceptable.

Now looking at the third variable R_i and considering equation (3.17) we can easily that R_i is to be chosen as small as possible to minimize F_{act} for clockwise rotation. Several values of R_i are evaluated where the maximal value for R_i is considered to be half the arm length. A gear larger then half the arm length R_i would result in a transmission ratio larger than one between the ingoing shaft and the radial pulley shaft, which is not desirable. From gear calculations follows that the minimal value of R_i lies at about 28 mm since, considering the forces on the gear, a smaller gear would result in possible failure. The influence of varying r_i on the required actuation power however is fairly small.

Research by Jos d. Ouden [1] shows that a pre-reduction of 6 is required to give the radial pulley the right rotational speed. This means that R_i can be chosen freely to obtain the right transmission ratio in combination with a certain belt transmission connecting to either the flywheel of the crankshaft of the engine, resulting in a total pre-reduction of 6. Also different belt transmission ratios can be corrected by choosing r_i properly.

In Table 5.1 the optimized dimensions are presented, where R_i is chosen just as large as the radial pulley. Furthermore the dimensions are an indication for the actual design dimensions since there are still some unknown factors in the design, such as the diameter of the input shaft and consequently the required distance between the input shaft and the push belt.

R_i	= 30	[mm]	Radius at which the ingoing torque acts
L_{arm}	= 100	[mm]	Length of the actuation arm
a_{act}	= 240	[mm]	Arm pivot–axial pulley shaft distance
T_{act}	= 560	[Nm]	Maximal required actuation torque
P_{act}	= 350	[W]	Maximal required actuation power
w_{act}	= 0.64	[rad/s]	Maximal required angular shifting velocity

Table 5.1: Indications for optimized dimensions of the AR-CVT, maximal torque and power for these dimensions

Chapter 6

Actuator Alternatives

The actuation of the AR-CVT is preferably electro-mechanically. Conventional CVT's use hydraulic pressure to realize shifting, this is however a complex system using rotating seals, hydraulic manifold and valves and an external hydraulic pump. Electromechanical actuation is cheaper and much easier to produce and on top of that easier to control. In this chapter several alternative actuation systems, all using an electric motor to actuate, are analysed and compared. Important in this comparison is the safety feature which makes sure that if the actuation fails the AR-CVT automatically shifts down due to the forces in the belt and on the pulleys. This means that the actuation is preferably non-self-locking. Furthermore the alternatives are compared with respect to the supplied actuation power and torque, the hold torque they can generate without overheating or failing, the shift rate they can achieve and some constructive details. The comparison of the alternatives is represented in Table 6.

Alternative 1: spur gear transmission connected to the actuation shaft

At first glance the most simple solution seems an electric motor in combination with a spur gear transmission connected to the actuation shaft. Electric motors that can deliver the required power are very commonly used and commercially available at low cost. They can be small and operate at high velocities, guaranteeing sufficient shift rate. From the previous chapter emerged however, that the maximal required actuation/hold torque is about 560 Nm. To generate torques this large with an electric motor, without it weighing more than a few kilograms, requires a very large transmission ratio (order $r = 500$) between the motor and the actuation shaft. This requires a lot of construction space and a transmission of this magnitude is probably self-locking. On top of that, electric motors are very unsuited to deliver a large hold torque at very low shift rates. However if the transmission is self-locking this is not a problem because the required hold torque is then delivered by the transmission itself.

Alternative 2: worm gear connected to the actuation shaft

More or less the same principal as the one mentioned above is using an electric motor in combination with a worm gear connected to the actuation shaft. It has the same advantages as the first alternative i.e. it can deliver enough power and shift rate and it is cheap. In addition, the worm gear system is small compared to the first alternative, however it is per definition self-locking. This does mean it is able to deliver sufficient hold torque.

Alternative 3: spur gear transmission indirectly connected to the actuation shaft

A third possibility is using an electric motor in combination with a spur gear transmission connected to a curved rack attached to the actuation arm at a certain distance from the actuation shaft. The electric motor generates sufficient power and shift rate. By choosing this distance larger than the actuation arm length it is possible to decrease the actuation torque and in addition it can be decreased by choosing the right gear transmission. However if you choose the distance between the rack and the actuation shaft twice the arm length it still requires a very large transmission ratio and moreover it becomes a very impractical solution considering the size and manufacturability. It might even result in a self-locking transmission and again the electric motor is unsuited to provide a large torque at very low shift rates.

Alternative 4: lead screw fixed at an offset from the actuation shaft

A different type of electric motor can be used to actuate the arm at a certain distance from the actuation shaft. A lead screw is a device which can deliver a lot of force in the longitudinal direction. They have small dimensions and are easy to build in. The required power might however be a problem since either the velocity in longitudinal direction is very low for commercially available lead screws. It is possible to obtain lead screws with larger longitudinal velocities but this means a decrease in axial load-taking capacity. Thus either the velocity or the force is to low.

Alternative 5: electromechanically braked actuation

Another solution for the problem of being unable to supply sufficient force at practically zero shift rates is mounting a brake to the actuation shaft. One might be able to compensate for the large required hold torque. However from Chapter 4 it appears that on a European Transient Cycle, the shift rate is hardly ever completely zero. Depending on the allowable margin in the shift rate, this means the brake is hardly ever closed, rendering the alternative obsolete. However one might consider a solution with a slipping brake which, due to a clever control system, does

not interfere with the actuation. This is a rather complex solution considering the required controllers, losses in due to friction and hysteresis but it is not dependent on extra external sources. At least not an electromechanical brake, for a pneumatic brake gives the same manufacturability problem as alternative 6. Also this alternative still needs a large gearing which might appear self-locking resulting in the problem mentioned before.

Alternative	Power	(hold) Torque	Shift Rate	Self-locking	Size	Cost	Manufacturabillity
Spur gear (s.g.)	$+$	$--$	$++$	$-$	$++$	0	$++$
Worm gear	$+$	$++$	$+$	$--$	$+$	$++$	$+$
s.g. on rack	$+$	$-$	$+$	$-$	$-$	0	0
Lead screw	$--$	$++(--)$	$--$	$--(++)$	$+$	$++$	$++$
Brake & s.g.	$+$	$++$	$+$	$-$	0	$-$	0

Table 6.1: Properties of several actuation design

Chapter 7

Conclusions and Recommendations

A simplified model depending on geometry and based on the required outputs is presented in this report. However the assumptions made to simplify a complex CVT model appearers to result in significant differences in outcomes. These differences nevertheless are found mainly in the numerical values of the calculated variables. The principle of the model holds and the dependance on geometry and load isn't compromised. Because of this an analysis could be made of the AR-CVT with the current list of demands, resulting in an overview of the specifications of the actuation system. Also these requirements can be recalculated for every change in the list of demands i.e. in designing future AR-CVT applications the presented method could be used with a different list of demands.

Based on the European Transient Cycle the required actuation power has been calculated and it doesn't impose any insurmountable obstacles in the principle of an electronically actuated AR-CVT. The required power is about the same as the currently required actuation power for a system with half the capacity.

A geometrical optimum has been found an it is shown that the direction of rotation of the system is of great influence to the specifications of the actuation system.

The design of the actual actuation requires more research. Two requirements seem to counteract one another since there is a large hold torque required at very low shift rates which is very difficult to achieve with electric motors if a self-locking actuation is not preferable.

Furthermore the model itself can be expanded and made more accurate and versatile by implementing more complex methods of calculating torque and clamping force build-up. Especially the negligence of some forces, for instance the internal belt forces, can be re-evaluated resulting in a more accurate model. Hereto different assumptions have to be made resulting in more profound calculation methods without losing the benefits of a simple and direct designing tool for AR-CVT applications.

List of Figures

List of Tables

Bibliography

[1] Den Ouden, Jos H.V.; *Feasibility study for the AR-CVT concept within the CS-PTO concept*; Technische Universiteit Eindhoven, Eindhoven, report number: DCT-2005/24

[2] Van Leeuwen, Harry; *Principes van Mechanische Componenten*; Technische Universiteit Eindhoven, Eindhoven

[3] Vroemen, Bas G.; *Component Control for the Zero Inertia Powertrain*; Technische Universiteit Eindhoven, Eindhoven, ISBN: 90-386-2593-6